380

Clear-sky window channel radiances: a comparison between observations and the ECMWF model

Isabel F. Trigo[1] and Pedro Viterbo

Research Department

October 2002

[1] Instituto de Meteorologia / Centro de Geofísica
da Universidade de Lisboa, Lisbon, Portugal

Submitted to J. Appl. Meteor.

For additional copies please contact

The Library
ECMWF
Shinfield Park
Reading, Berks RG2 9AX

library@ecmwf.int

Series: ECMWF Technical Memoranda

A full list of ECMWF Publications can be found on our web site under:
http://www.ecmwf.int/publications.html

Abstract

A comparison of clear-sky radiances of the Meteosat window channel with ECMWF (European Centre for Medium-Range Weather Forecasts) model results is presented, aiming to assess both the model's performance and the quality of the observations. The comparison is made for four periods covering the seasonal cycle and for the Meteosat-7 (Africa and Southern Europe) and the Meteosat-5 (Middle East and the Indian subcontinent) disks. Results show an underestimation of the diurnal cycle of model brightness temperature in clear-sky conditions with a cooling error during daytime of up to 7-8 K, and a much smaller and less widespread warming error at night. Although such discrepancies are sensitive to surface characteristics (e.g. vegetation type, terrain elevation, and slope), problems in the model surface-to-boundary-layer coupling are identified as the most likely model deficiency associated to the underestimation of diurnal amplitudes of skin temperature. A conditional error analysis also reveals strong error stratification with the model cloud cover and with the percent of clear-sky pixels associated with the Meteosat data, suggesting great care should be taken when using Meteosat clear-sky observations, particularly in the ITCZ and adjacent areas.

1. Introduction

The past two decades have seen an increased usage of remote sensing observations by many operational data assimilation systems, including ECMWF's (European Centre for Medium-Range Weather Forecasts). Observations from instruments on polar orbiting platforms, such as the infrared (IR) and microwave channels of the TOVS (TIROS Operational Vertical Sounder) suite of instruments, are crucial to the quality of current analyses (Bouttier and Kelly 2001) and a major contributor to the improvement in the quality of forecasts (Simmons and Hollingsworth 2002). Efforts are underway to improve the usage of observations from geostationary satellites, such as GOES (Geostationary Operational Environmental Satellite) and Meteosat, operated by the European organization for the Exploitation of Meteorological Satellites (EUMETSAT) (Rohn et al. 2001, Munro et al. 2000).

Effective usage of remote sensing information for Numerical Weather Prediction (NWP) requires a good quality background field. In particular, the remote sensing channels that peak at the lower troposphere require a good a-priori knowledge of the surface skin temperature. Over sea, the sea surface temperature (SST) is determined using a combination of visible imagers and buoys, with an accuracy better than 0.5 K (Reynolds and Smith 1994). The model skin temperature over land is a much more elusive quantity, due to several effects: (a) the fast response (low thermal inertia) of the land surface temperature; (b) the sensitivity of the skin temperature to local effects (such as terrain characteristics, land cover, vegetation state), which are imperfectly described by the ancillary datasets of the land surface parameterization scheme; (c) the imperfections of the model's physical parameterizations, leading to large uncertainties in the accuracy of the model soil water, or of the model thermal roughness lengths (e.g., Sun and Mahrt 1995), in turn affecting the skin temperature.

The current ECMWF land surface parameterization scheme, TESSEL (Tiled ECMWF Scheme for Surface Exchanges over Land) (van den Hurk et al. 2000), has up to six independent fractions (tiles) for every land grid box, with separate skin temperatures and fluxes. Each tile has its own characteristics defining separate heat and water fluxes used in an energy balance equation solved for the tile skin temperature. One of the long-term goals for designing TESSEL was a better usage of remote sensing information. So far there has been limited validation of the skin temperature in global models, despite the obvious importance of skin temperature in (a) determining the surface sensible heat flux (Hall et al. 1992; Sun and Mahrt 1995), (b) computing the evaporative fluxes using the so-called big-leaf approximation (as reviewed in Dickinson et al.

1991, and Sellers et al. 1997; see also Deardorff 1978; Dickinson et al. 1993; Sellers et al. 1996; Viterbo and Beljaars 1995; van den Hurk et al. 2000), and (c) estimating soil water from microwave radiances (e.g. Wang et al. 1992) or IR radiances (e.g. McNider et al. 1994).

Two recent studies compare skin temperatures in large-scale models with derived remote sensing information. Jin et al. (1997) focus on the skin temperatures of the National Center for Atmospheric Research (NCAR) Community Climate Model version 2 (CCM2) coupled with the BATS (Biosphere-Atmosphere Transfer Scheme) surface model. Data from a 10-year simulation at T42 spectral resolution are compared with one year data retrieved from the High Resolution IR Radiation Sounder (HIRS) on TIROS-N in 1979, and with FIFE (First ISLSCP Field Experiment) skin temperature observations in July 1987. HIRS retrievals of observed skin temperatures are obtained from radiances for the night-time (0300 LT) and daytime (1500 LT) overpass, while the FIFE data is an average of observations taken every 5 min with 22 IR thermometers mounted at 3-m above surface and distributed over the FIFE area. Rhoads et al. (2001) compared the output of a suite of off-line surface models in the Red-Arkansas River basin in the Southern Great Plains with hourly data obtained from the HIRS instruments for the night-time and daytime overpass and data from the window channel of the GOES satellite. HIRS-2 skin temperature was compared with three large-scale Northern Hemisphere field experiments sampling different ecosystems and climates, for several years. The data was found to be bias-free with a 4-5 K standard deviation.

We report a pilot study on the use of clear-sky radiances of Meteosat 11μm window channel for the assimilation of land surface temperature. As a first step towards assimilation, Meteosat clear-sky radiances are compared with their model equivalent (Köpken et al. 2002). Analysis of the differences between observed and modeled clear-sky radiances enables one to assess the quality of the modeled land surface temperature, and particularly its diurnal cycle. In clear-sky conditions, the model's outgoing radiance depends essentially on the surface or skin temperature, which is calculated from the energy budget at the surface. The comparison serves not only to assess the model's performance, but also to monitor the quality of the observations by identifying gross errors or systematic problems in the data.

A description of the data and methodology used is presented in Section 2. Section 3 starts with an overview of the mean fit of the model to the observations, followed by focusing on the time variability and stratification of results by surface type, and finally the characterization of the conditional bias. Section 4 discusses possible reasons for the large observed biases, and suggests practical ways of overcoming the problems, while the major conclusions are reviewed in the final section, highlighting areas where future work is needed.

2. Data and Methodology

This study is focused on the comparison between radiances measured by the infrared (IR) window channel (10.5 – 12.5 mm band) on-board Meteosat-7 and Meteosat-5, and their ECMWF model equivalent. The study is performed for four 15-day periods in 2001 – 1-15 February, 1-15 April, 1-15 July, and 1-15 October – sampling the annual cycle within the Meteosat-7 disk (centered at 0ºE) and Meteosat-5 disk (centered at 63ºE).

2.1 Observations

Meteosat radiances are used here in the form of so-called clear-sky radiances (CSR) produced by EUMETSAT (van de Berg et al. 1995). To derive the CSR, the observed radiances are screened for clouds at EUMETSAT. This is done through a cluster analysis over 32x32 pixel segments using the available channels, i.e. 11 μm and 6.3 μm at night, while during daytime the visible channel is used in addition. The individual clusters may then be classified into clear land/sea and scenes with different cloud heights by comparing the cluster mean values to calculated radiances. These are based on radiative transfer calculations using ECMWF short-range forecast profiles and surface temperatures. The observed CSR, hereafter Tb_obs, are obtained by averaging the values diagnosed as "clear sky" within the four 16x16 quadrants in the segments. The original spatial image resolution of 5 km is thus degraded to about 80 km at nadir, and to about 125 km at 50ºN. Along with the averaged clear-sky radiances, the percent of pixels flagged as "clear sky" and as "cloudy" are also given by EUMETSAT. Although the CSR data are produced hourly, only 3-hourly brightness temperatures will be compared with their ECMWF model equivalent. Clear-sky radiances are affected by calibration errors that are satellite dependent, further discussed in Section 4 of the paper (see also Köpken et al. 2002).

2.2 Modeled Brightness Temperatures

The modeled brightness temperatures are obtained from the ECMWF background fields presented to the data assimilation scheme – a 4-dimensional variational assimilation (4D-Var) (Rabier et al. 2000; Mahfouf and Rabier 2000; Klinker et al. 2000). The model version is the so-called 23r4 cycle, tested since November 2000 and operational since June 2001, running at T511L60 (60 levels with a horizontal grid spacing of about 40 km). The derivation of the analysis increments in the12-hour 4D-Var (Bouttier 2001) is performed at T159L60 (corresponding to a grid spacing of about 125 km). The 3-hourly model background fields used here have verifying times between 18 UTC and 3 UTC for the 0 UTC analysis, and between 6 UTC and 15 UTC for the 12 UTC analysis.

Although Meteosat 11 μm radiances are not currently being assimilated at the ECMWF, the background window channel brightness temperatures (Tb_bg) are obtained using the background profiles of temperature and humidity, the skin temperature, and the specified surface emissivity as input to the Radiative Transfer for TOVS model version 5 (RTTOV-5) (Eyre 1991; Saunders et al. 1999). The model cloud cover, liquid and ice water are ignored in the radiative transfer, and thus the Tb_bg provided are always considered clear-sky. A basic description of RTTOV follows, in order to discuss the possible error sources associated with Tb_bg.

The atmospheric upwelling clear-sky radiance, $L^{clr}(\nu,\theta)$, at frequency ν and viewing angle θ from zenith at the surface is written as:

$$L^{clr}(\nu,\theta) = \tau_s(\nu,\theta)\varepsilon_s(\nu,\theta)B(\nu,T_s) + \int_{\tau_s}^{1} B(\nu,T)d\tau + (1-\varepsilon_s(\nu,\theta))\tau_s^2(\nu,\theta)\int_{\tau_s}^{1}\frac{B(\nu,T)}{\tau^2}d\tau$$

where the first term is the radiance emitted by the surface, the second term is the direct radiance emitted by the atmosphere and the third is the radiance reflected by the surface; τ_s and τ are the surface to space and the layer to space transmittances, respectively, ε_s is the surface emissivity, B is the Planck radiance for a scene temperature, and T and T_s are the layer mean temperature and the surface skin temperature, respectively.

$L^{clr}(v,\theta)$ is convolved with the instrument filter function (different for Meteosat-7 and Meteosat-5) to give the actual channel radiance.

In the remaining part of the paper we will be linking the mismatch between model and observed brightness temperatures to problems in the observation data and deficiencies in the model skin temperature, in particular its diurnal cycle. It is clear from the equation above that there are other factors that might affect the model radiances, besides the surface skin temperature, and they are summarized here. First, the formulation of the window channel emissivity is rather crude: land emissivity is set everywhere to 0.96, except in very dry areas where it can reach values as low as 0.93 (see more details in section 4). Tests with alternative formulations of emissivity have shown an impact on Tb_bg of order 1 K, but no impact on its diurnal cycle. Secondly, deficiencies in the atmospheric water vapor affect the atmospheric transmissivity. Since the diurnal cycle of the total column water is small, the impact on the diurnal cycle of Tb_bg is less than 1 K (Chevallier and Kelly, 2002). An additional factor impacting the atmospheric transmissivity is the aerosols, with impact on Tb_bg less than about 1 K, and even smaller on its diurnal cycle. Finally, deficiencies in the RTTOV radiative transfer can lead to biases and standard deviations of Tb_bg of order 0.1 K (Matricardi et al. 2001).

2.3 The land surface model TESSEL

The model skin temperature is largely determined by the details of the land surface model used, TESSEL (van den Hurk et al. 2000). TESSEL conceptually divides the surface/atmosphere interface into fractions (tiles), with up to 6 tiles over land (bare ground, low and high vegetation, intercepted water, shaded and exposed snow) and up to 2 fractions over sea and freshwater bodies (open and frozen water). Each fraction has its own properties defining separate heat and water fluxes used in the energy balance equation that is solved for skin temperature. Special attention is devoted to the different physical mechanisms limiting evaporation over bare ground and vegetated surfaces. Over land, the skin temperature is in thermal contact with a four-layer soil or, if there is snow present, a single layer snow mantle overlying the soil. In this study we will be using only the weighted average skin temperature over the grid box. However, future use of specific remote sensing instruments might be dealt with more appropriately with a given tile temperature rather than the grid box average.

2.4 Methodology

Background departures (BG_dep), i.e., the difference observed minus collocated modeled brightness temperatures, were studied taking into account a set of model variables and parameters also collocated to each Tb_obs value. The results presented here concern the stratification of the BG_dep by the model surface type and vegetation, a fixed parameter based on the Global Land Cover Climatology (Loveland et al. 2000; van den Hurk et al. 2000), and by the modeled cloud cover. The latter, classified as low, medium or high, is obtained by the cloud prognostic scheme developed by Tiedke (1993) with modifications described by Jakob (1999), Jakob and Klein (2000), and Jakob et al. (2000).

In section 3, a general overview of the BG_dep over the Meteosat-7 and Meteosat-5 disks will be presented. This will be followed by a more detailed analysis of the diurnal cycle of the BG_dep over a set of previously chosen areas (Fig. 1, Table 1), most of the order of 10ºx10º. Although only inland regions are of interest for the present study, the selection of those areas follows quite closely the criterion used by Morcrette (1991). Here a set of inland areas was selected so that at each time-slot the atmospheric conditions within each

region are fairly homogeneous. As for the surface type, some areas are fairly homogeneous - regions M7-3, M7-4, M7-7 -, while others display a marked north-south gradient – as in regions M7-5 and M7-6.

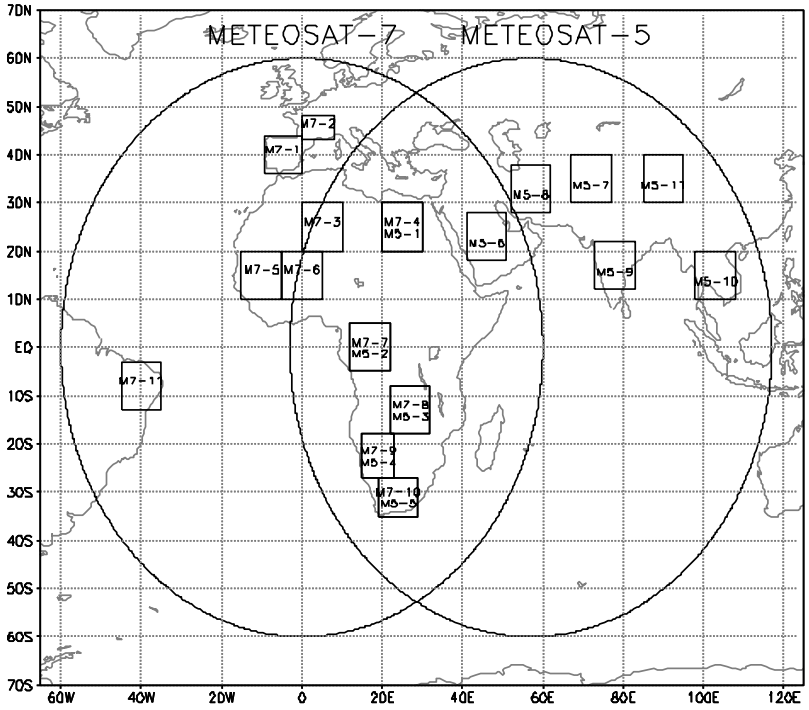

Figure 1 Areas studied within Meteosat-7 (M7-n) and Meteosat-5 (M5-n) disks.

Meteosat-7		**Meteosat-5**	
M7-1 Iberia	9.5 W – 044 N – 36 N	M5-1 Egypt	20 E – 30 E30 N – 20 N
M7-2 France	0 – 8 E48 N – 43 N	M5-2 Congo	12 E – 22 E5 N – 5 S
M7-3 W. Sahara	0 – 10 E30 N –20 N	M5-3 Savannah	22 E – 32 E8 S – 18 S
M7-4 Egypt	20 E – 30 E30 N – 20 N	M5-4 Namibia	15 E – 23 E18 S – 27 S
M7-5 Mali	15 W – 5 W20 N – 10 N	M5-5 S. Africa	19 E – 29 E27 S – 35 S
M7–6 Niger	5 W – 5 E20 N – 10 N	M5-6 Arabian P.	41 E – 51 E28 N – 18 N
M7-7 Congo	12 E – 22 E5 N – 5 S	M5-7 Himalayas	65 E – 77 E40 N – 30 N
M7-8 Savannah	22 E – 32 E18 S – 8 S	M5-8 Mid. East	52 E – 62 E38 N – 28 N
M7-9 Namibia	15 E – 23 E18 S – 27 S	M5-9 India	73 E – 83 E22 N – 12 N
M7-10 S. Africa	19 E – 29 E27 S – 35 S	M5-10 Indochina	98 E – 108 E20 N – 10 N
M7-11 Brazil	45 W – 35 W3 S – 13 S	M5-11 Mongolia	85 E – 95 E40 N – 30 N

Table 1 Studied areas within Meteosat-7 and Meteosat-5.

3. Results

3.1 Overview

The BG_dep (observed minus modeled brightness temperatures) averaged for each of the 15-day periods are shown in Figs. 2-5. The 3 UTC (0UTC) and 12 UTC (9 UTC) time-slots are representative of the night and daytime periods for the Meteosat-7 (Meteosat-5) disk, respectively. Using the local midnight was avoided due to problems caused by the so-called solar stray light effect, which happens when solar light intrudes into the radiometer producing spurious bright spots and bows (Köpken 2001).

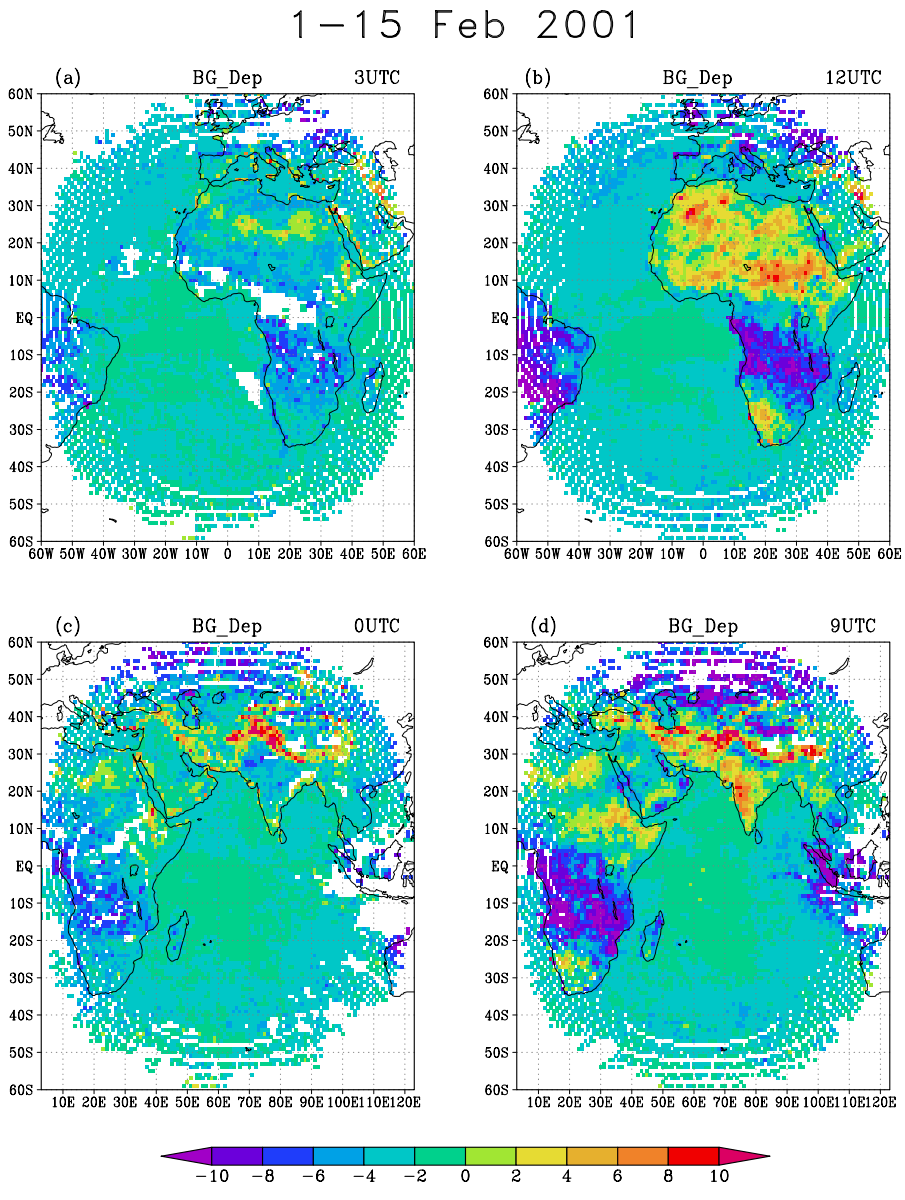

Figure 2 BG_dep (K) averaged for the period 1-15 February 2001 obtained for Meteosat-7 at (a) 3 UTC and (b) 12 UTC, and for Meteosat-5 at (c) 0 UTC and (d) 9 UTC.

The differences between observed and modeled brightness temperatures for the night time BG_dep generally range from –4K to 4K; over the Himalayan mountains the night time bias may reach up to 10 K (Figs. 2c, 3c, and 5c), associated to an overestimation of the model cooling over such high elevated terrain.

The BG_dep mark very distinctly the land-sea border, during daytime, with BG_dep between –2K and –3K, close to the calibration uncertainty (van de Berg et al. 1995), over the oceans remaining fairly constant throughout the day. These values are consistent with the findings of Köpken et al. (2002), who studied the background departure statistics for 100% clear-sky data and found a bias of –2K to –2.8K, with standard deviations of 1K, for Meteosat-7 and Meteosat-5, respectively. The inland negative (positive) nighttime bias are enhanced at 12UTC (Figs. 2b-5b) and 9UTC (Figs. 2d-5d). The February 12 and 9 UTC time-slots (Figs.

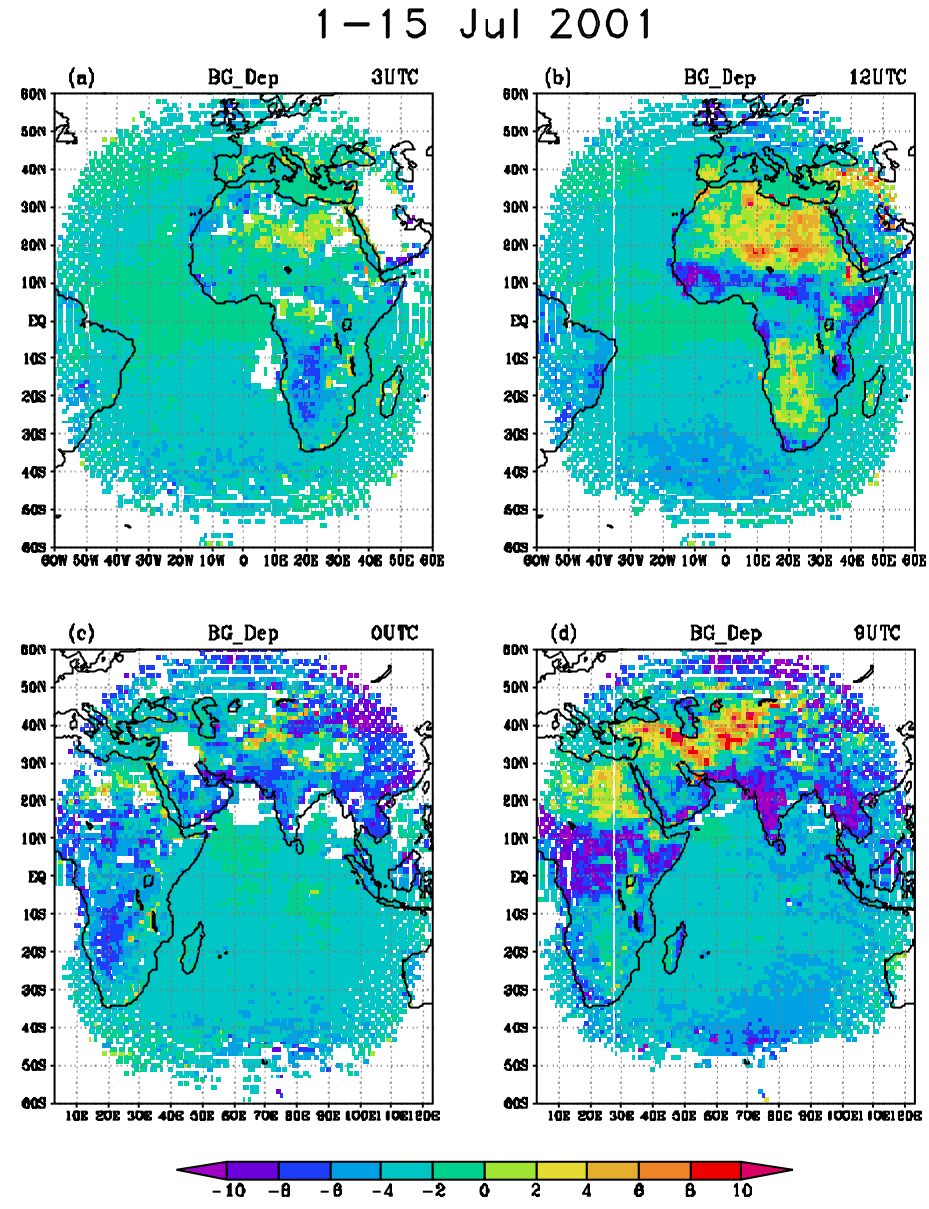

Figure 3 As in Fig. 2, but for the period 1-15 April 2001.

2b and 2d) show large areas where positive BG_dep clearly dominate; these include most of the semi-arid and desert African regions – the Sahara, the Sahel and the Namibia desert – most of the Middle East – the latitudinal band between Turkey and Pakistan – and India. Over these regions the modeled brightness temperatures at or near their diurnal maximum tend to be colder than the observations by 2K to over 8K. Since model clear-sky radiances for the window channel are mainly driven by the surface temperature, Figs. 2b and 2d show vast areas where the amplitude of the modeled skin temperature is systematically underestimated, a problem also reported by Morcrette (2002), when comparing model values of skin temperature with ground-based observations over the Atmospheric Radiation Measurement Southern Great Plains site.

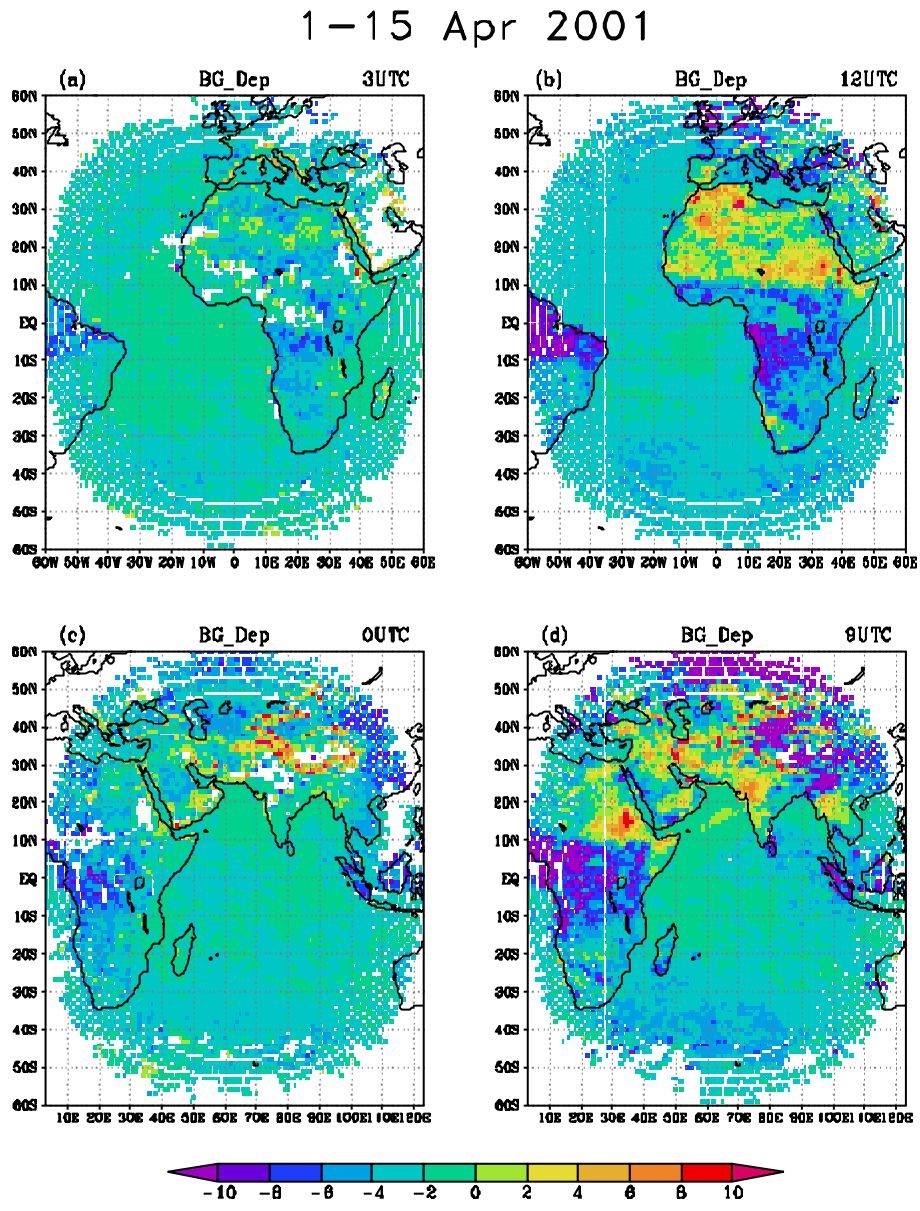

Figure 4 As in Fig. 2, but for the period 1-15 July 2001.

The corresponding regions with strong daytime negative bias for February 2001 are mainly constrained to the 0º – 20ºS latitudinal band (Figs. 2b and 2d). For the next months the daytime negative values of the BG_dep, mainly between 10ºS and 20ºS, weaken (Fig. 3b) and are replaced by a positive bias over southern Africa in July (Fig. 4b) and October (Fig. 5b). Meanwhile, the negative BG_dep band has moved northwards following the intertropical convergence zone (ITCZ) and the onset of the monsoon in the Indian subcontinent, linking the main factors guiding the spatial distribution of the most pronounced negative/positive BG_dep patches in the subtropics to the local rainy/dry season. As further discussed in Section 4, these may be related either to the observations, such as deficiencies in the cloud clearing, or to the

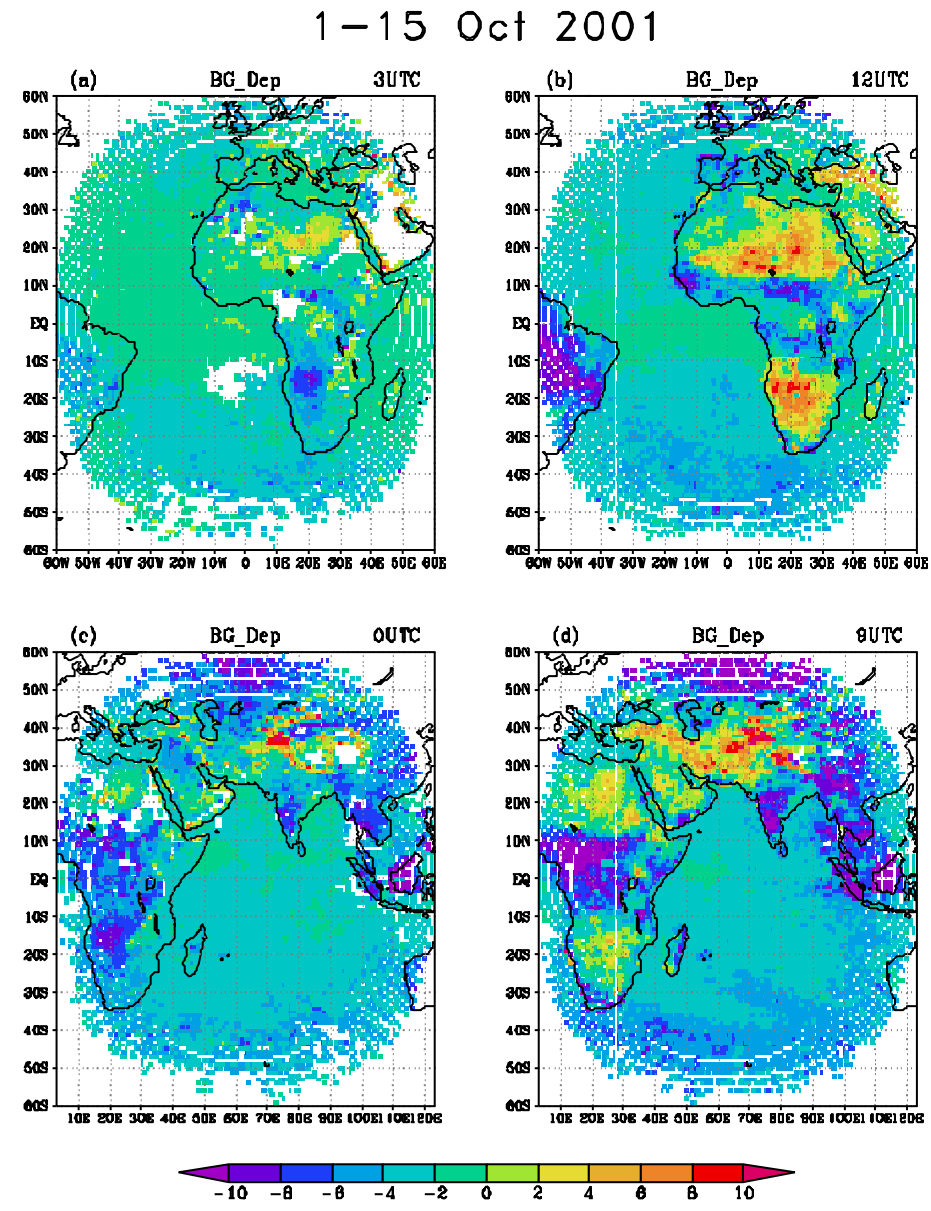

Figure 5 As in Fig. 2, but for the period 1-15 October 2001.

model, e.g., the inadequacy of climatologically fixed model parameters, such as albedo, vegetation cover and type, or model variables, such as soil moisture, humidity profiles / total water vapor content.

The patterns of the BG_dep averages over areas with superposition of Meteosat-7 and Meteosat-5 disks are similar (e.g., Figs 2a and 2c, 2b and 2d), although the average BG_dep tend to be lower for Meteosat-5 disk than for the same inland areas within the Meteosat-7. The averaged values of the BG_dep for some of those areas are shown in Fig. 6. Joyce et al. (2001) point to a number of effects that might explain the discrepancies between the two satellites: the non-uniform distribution of undetected cloudiness and the different viewing angles, in this case higher for Meteosat-5, which contribute for lower Tb_obs for the eastern satellite. Both effects tend to be more pronounced in the tropics, in accordance with the higher discrepancies found for the Congo area; the diurnal and seasonal cycle of the temperature contrast between the land surface and the tropopause may explain the higher differences during day-time, particularly over dry areas (see e.g. Egypt, and South Africa in February and October, Fig. 6), as well as their annual fluctuations.

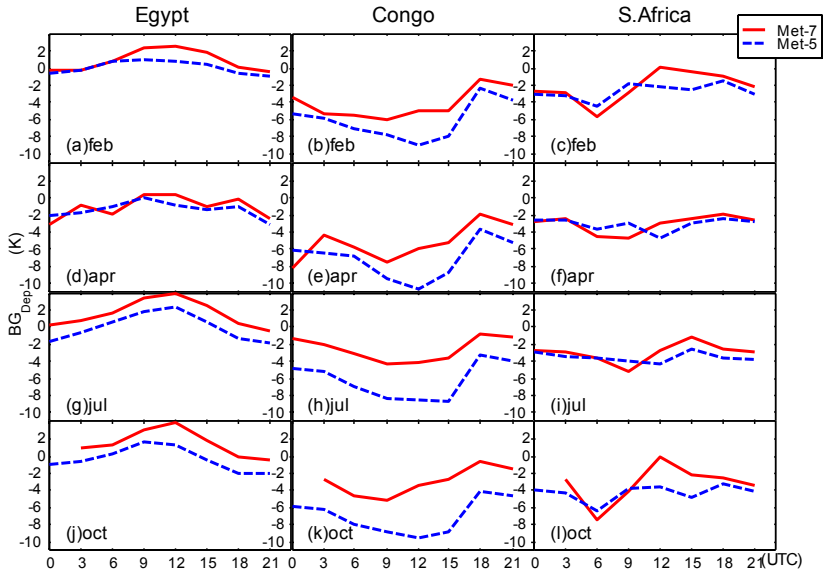

Figure 6 BG_dep (K) for three areas (Egypt, Congo and South Africa) with superposition of Meteosat-7 and Meteosat-5 disks, averaged every 3-hours over 15-days period in February (1st row), April (2nd row), July (3rd row), and October (4th row).

Although Figures 4b and 4d do not correspond to the same observation times, they are also indicative of the spatial distribution of the main differences between the two satellites; positive BG_dep in the latitudinal band from 5ºS to 30ºS in the Meteosat-7 disk (Fig. 4b) is replaced by weaker values in Fig. 4d, while the negative values of the BG_dep around 10ºN in Fig. 4b are more pronounced and extend further south in Fig. 4d. The corresponding pictures for October (Figs. 5b and 5d) follow a similar pattern. Although the respective viewing angles are taken into account by RTTOV-5 for the computation of the atmospheric correction, the effects discussed above (Joyce et al. 2001) are probably not totally eliminated. However, a significant fraction of the discrepancies found for the two satellites is likely to be accounted by differences in the spectral responses, and in the calibration of the respective on-board radiometers. For Meteosat-5 the so-called vicarious calibration is used (Köpken 2001; van de Berg et al. 1995), while the black body on-board Meteosat-7 is being used for its calibration since May 2000 (Köpken 2001; Tjemkes et al. 2001).

3.2 Temporal Variability

In order to identify the main sources of systematic errors of Tb_bg, the BG_dep were analyzed for each of the regions defined in Table 1 (Fig. 1). The time-series of the BG_dep for Niger (Meteosat-7 data), Congo (Meteosat-7 data), and Himalayas (Meteosat-5 data) are plotted in Fig. 7 for the February period. The northern African regions under the influence of the subsidence branch of the Hadley cell, including the Niger limited area (Fig. 7a) are characterized by dry atmosphere and very low soil moisture. The high proportion of coherent diurnal variability of the observed and modeled brightness temperatures (Morcrette 1991) seems to be also mirrored in the diurnal fluctuations of the BG_dep (Fig. 7a). Over dry regions, the top of atmosphere brightness temperatures for the window channel are mostly driven by the surface, and thus indirectly by surface properties. Some stratification of the BG_dep values seems to be associated with the respective dominant vegetation type (legend to the right of each panel in Fig. 7), e.g., for the Niger area, the higher maximum daily values of the BG_dep tend to be reached for the "Tall Grass" type. However, care must be taken in the analyses of such results since, given the North-South gradient of vegetation type, at least part of the stratification by surface characteristics reflects latitudinal variation in the atmospheric conditions. This effect may be particularly pronounced for the Congo area (Fig. 7b), where the types "Evergreen Broadleaf Trees" and "Deciduous Broadleaf Trees" are more likely to be under the influence of the ITCZ than the points characterized by "Interrupted Forest", generally located toward the north of the region. For the former vegetation types, the daytime brightness temperatures are often overestimated by 15K or 25 K by the model. Known deficiencies in the model humidity profiles in the tropics (Marécal et al 2001; Marécal and Mahfouf 2002), associated with underestimation of the total water vapor column, may be responsible for an inadequate atmospheric impact on the brightness temperatures. However, the Tb_bg errors associated with humidity profiles are likely to be within ±2K range (Chevallier and Kelly 2002).

Within the studied regions, the time-series for the Himalayas limited area (Fig. 7c) exhibits the highest dispersion of the BG_dep around the mean for each time-slot. There, the stratification by vegetation type reflects mainly the local orography. Over the most elevated terrain, where "tundra" and "short-grass" vegetation types dominate, brightness temperature is grossly underestimated by the model, with BG_dep of the order of 20 K and over. In contrast with all the other studied areas, the high dispersion of the BG_dep occurs for both daytime and night. Again, this is likely to be associated with the local heterogeneous terrain, and to the smoothing of Himalayan topography in the model, with daily time-series for points corresponding to different heights and different slopes being overlapped; this effect seems to be particularly pronounced for the semi-desert type, the most common in the area (36% of the points).

3.3 Conditional Bias

For most studied areas, the BG_dep are strongly linked to the observed values of brightness temperature, i.e., the BG_dep have strong conditional bias. In this section we will show that the relation between the BG_dep and Tb_obs may be partially explained by other model variables, particularly by the modeled cloud fraction and cloud type. Moreover, the stratification of the time-series of BG_dep by vegetation type (and thus by surface type and albedo) discussed in the previous section (Fig. 7) may in fact underlie the spatial distribution of cloud cover and cloud type.

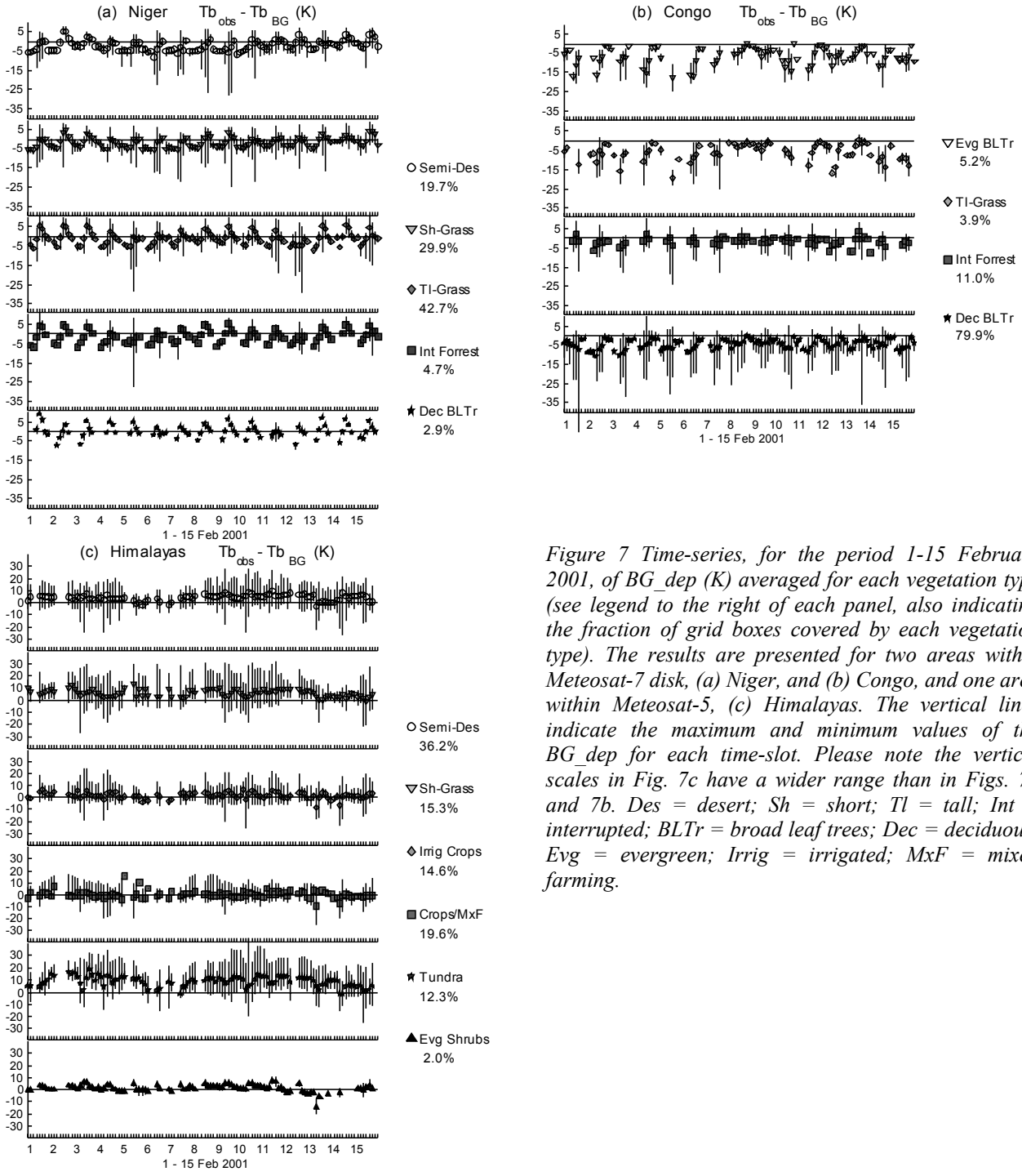

Figure 7 Time-series, for the period 1-15 February 2001, of BG_dep (K) averaged for each vegetation type (see legend to the right of each panel, also indicating the fraction of grid boxes covered by each vegetation type). The results are presented for two areas within Meteosat-7 disk, (a) Niger, and (b) Congo, and one area within Meteosat-5, (c) Himalayas. The vertical lines indicate the maximum and minimum values of the BG_dep for each time-slot. Please note the vertical scales in Fig. 7c have a wider range than in Figs. 7a and 7b. Des = desert; Sh = short; Tl = tall; Int = interrupted; BLTr = broad leaf trees; Dec = deciduous; Evg = evergreen; Irrig = irrigated; MxF = mixed farming.

At this point it should be stressed that the model clouds are ignored in the radiative transfer model RTTOV-5, which computes the difference between the modeled skin temperature and Tb_bg from temperature and humidity profiles. However, the model cloud fraction and cloud type still have a significant impact on the model radiative budget at the surface, and thus on the modeled skin temperatures.

Figure 8 shows the BG_dep values plotted against the respective Tb_obs for the "Western Sahara" limited area; each point is colored according to the model total cloud fraction (Fig. 8a and 8b) and the fraction of high clouds (Fig. 8c and 8d). There is a marked stratification of the BG_dep by the forecasted cloud cover; this effect is particularly pronounced for 12 UTC (Fig. 8b and 8d), and although not shown, is equally strong for 15 UTC, with 9 UTC (18UTC) being characterized by a slow transition from (to) the night period (Fig. 8a and 8c). The model cloudy points mark the two tails of (mostly) negative BG_dep (Fig. 8b); furthermore, the lower tail seems to be associated with the presence of high clouds (Fig. 8d) and, thus, the upper tail will correspond to low-to-medium clouds.

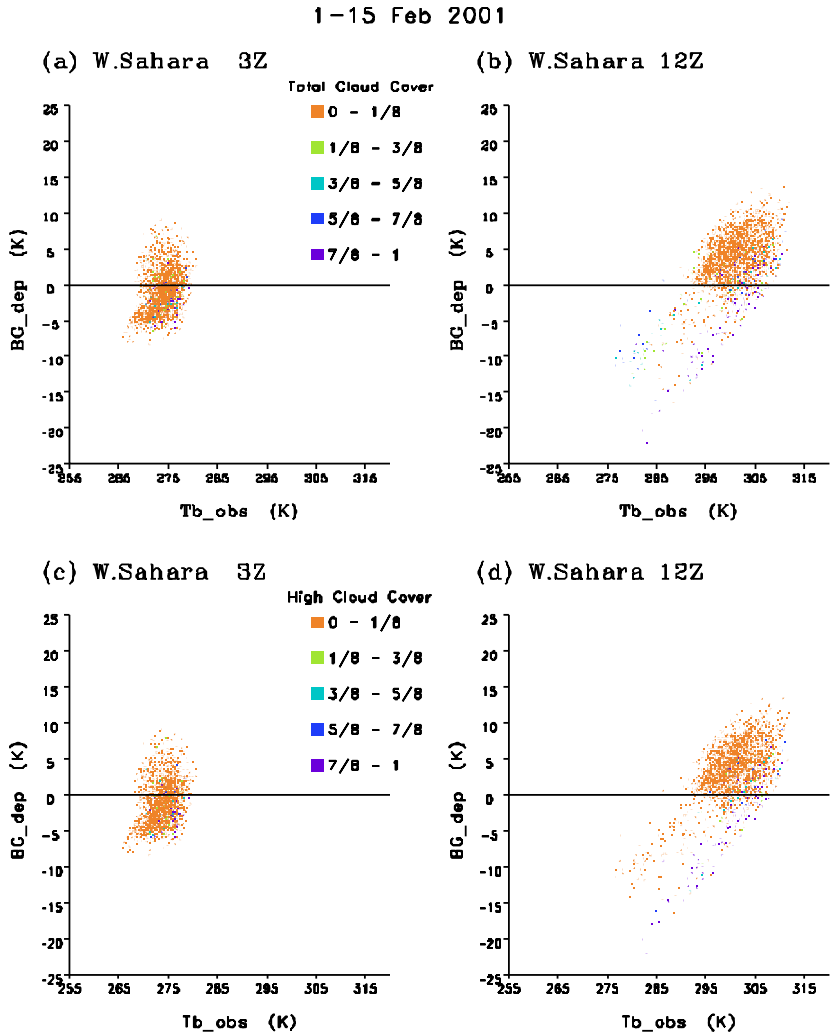

Figure 8 Scatterplots of the BG_dep (K) against Tb_obs (K), for the Western Sahara area, at 3 UTC and 12 UTC, as indicated in the top of each panel. The points are colored according to the forecasted total cloud cover - (a) and (b) – and forecasted high cloud cover – (c) and (d).

The BG_dep corresponding to clear-sky points (forecasted total cloud fraction below 0.125) in Figs. 8a and 8b, have an overall positive bias. The discrepancies between observed and modeled brightness temperatures grow steadily between night time, with averaged BG_dep of the order of –0.5 K found for clear-sky conditions at 00 UTC, to daytime with maximum BG_dep of the order of 4.5K at 15 UTC (not shown). The plots in Fig. 8 put into evidence the inability of the modeled brightness temperatures to follow the observed diurnal cycle; for the dry conditions observed in the Sahara region, this means the diurnal cycle of the modeled skin temperature is generally underestimated. This is particularly the case when Tb_obs (and thus

the observed skin temperatures) is high, i.e., when the diurnal amplitude is also likely to be high. As a consequence, the daytime BG_dep are positively correlated with the observations, with correlation coefficients reaching 0.6 for daytime with forecasted clear-sky.

The Savannah limited area is under the influence of the ITCZ during the February 15-day period; cases with modeled total cloud cover below 3/8 are almost non-existent. In this area, the BG_dep are strongly associated with the observations; correlations of 0.9 are obtained for both 03 and 12 UTC (Figs. 9a and 9b, respectively). The Savannah plots match the "cloudy tails" observed in Fig. 8; although not shown, the distinction between high and low or medium clouds no longer exists, probably due to the different cloud layers being overlapped.

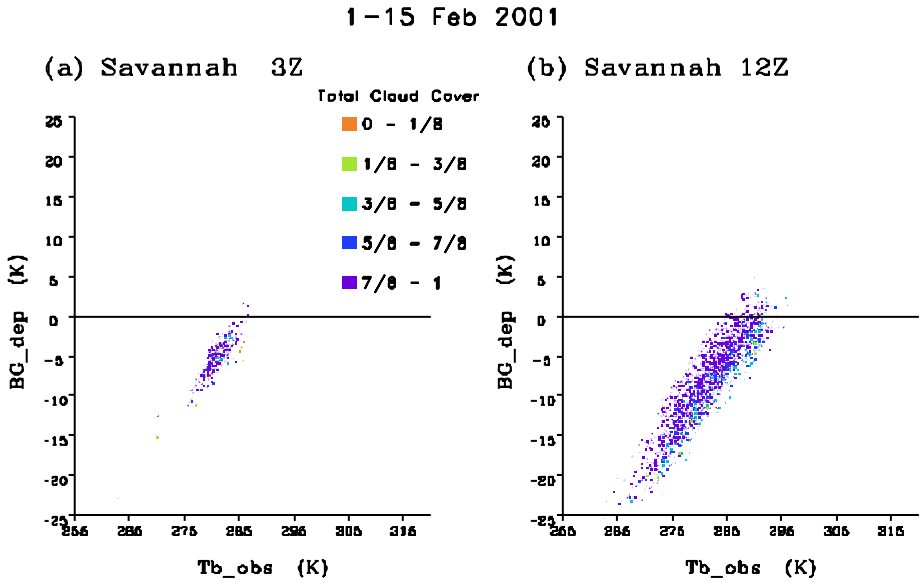

Figure 9 As in Fig. 8(a) and 8(b), but for the Savannah area.

4. Discussion

Over dry, clear-sky regions, the atmosphere is fairly transparent for the window channel. Consequently, the discrepancies between the modeled and observed brightness temperatures to a large extent reflect how well the skin temperature is simulated by the ECMWF model; furthermore, the diurnal variations of the BG_dep give a good indication of how the diurnal cycle of the surface temperature is being reproduced. Over land, and under clear-sky conditions, the diurnal variations of the skin temperature are particularly sensitive to surface characteristics, such as surface type/vegetation, albedo, and slope (Jin et al. 1997), which partially explain the spatial variability of the BG_dep shown in Figs. 2-5 for the arid and semiarid regions, and the stratification by vegetation type seen in Fig. 7 (7a and 7c). In those cases, the daytime BG_dep tend to be higher for daytime than for the night period, i.e., the amplitude of the modeled skin temperature tends to be underestimated. The window channel emissivity values prescribed in the model comprise a very limited number of categories, ranging from 0.93 over very dry areas (deserts) to 0.98 over snow and 0.99 over water surfaces. Over most land grid points, emissivity is set to 0.96. Updated values for a wider variety of land cover types (e.g., Snyder et al. 1998) could reduce the Tb_bg offset, such as the bias of ~-3K obtained for nighttime BG_dep. However, preliminary sensitivity studies have shown that the adjustment of emissivity values has a negligible impact on the amplitude of Tb_bg, which can only be accounted for by deficiencies in

the modeled diurnal cycle of skin temperature. Over mostly dry regions the model skin temperature is being misrepresented, possibly due to inadequate coupling of the surface to air temperature and/or to overestimation of the daytime surface sensible heat flux.

Over both subtropical and temperate areas, the respective dry seasons are characterized by BG_dep values and daily fluctuations similar to those described above. When the ITCZ settles in subtropical areas, or during the mid-latitudes winter, the patterns of the BG_dep change dramatically; the modeled brightness temperatures become systematically overestimated; the balance between daytime and night BG_dep is negative, i.e., the diurnal cycle of the modeled brightness temperatures is over-estimated. Although only cloud free data are being analyzed here, it has been shown that the modeled cloud cover has a strong impact in the stratification of the discrepancies between modeled and observed brightness temperatures. Such results must be taken with care since the ECMWF model has known cloud deficiencies, particularly in areas affected by extratropical cyclones and in the tropics where the temporal variation of convection is not well represented over land (Jakob 1999; Chevallier and Kelly 2002; Chevallier et al. 2001). The percent of clear-sky pixels corresponding to each observation (hereafter %_ClearSky) give an indication of the cloudiness in the area. In the case of the Sahara (Fig. 10a), the two tails of negative BG_dep correspond mostly to observations with low %_ClearSky, which categorize the BG_dep in a similar way to that observed with the modeled cloud cover. For convective areas (e.g. Fig. 10b) and regions within the mid-latitudes storm-tracks (e.g. Fig. 10c), there is again a good agreement between low %_ClearSky, low Tb_obs and strong overestimation of the respective modeled clear-sky values. This suggests the %_ClearSky is measuring indirectly the probability of the observed brightness temperatures being contaminated by top of the cloud radiances.

The negative BG_dep could be associated with the distribution of the model humidity, since water vapor is the only significant absorbent for the 11 mm channel (e.g., Morcrette 1991). A strong impact, though, would only be expected in convective tropical regions, where maximum values of the vertically integrated water vapor are found (Chang et al. 1984). However, we still have to assess whether the behavior of the BG_dep in convective tropical and subtropical regions, and in the mid-latitudes winter is likely to be attributed to clear-sky observations being contaminated by clouds, or to inadequate modeled fields. To answer that particular question, the phase of the diurnal cycle of Tb_obs was analyzed for:

i) Points where the daytime BG_dep is lower than –5K and the respective modeled total cloud cover is higher than 0.5, which contain most of the observations suspected of being cloud contaminated;

ii) Points where the daytime BG_dep is positive and the respective modeled total cloud cover is lower than 0.5, which have the lower probability of having any cloud problems.

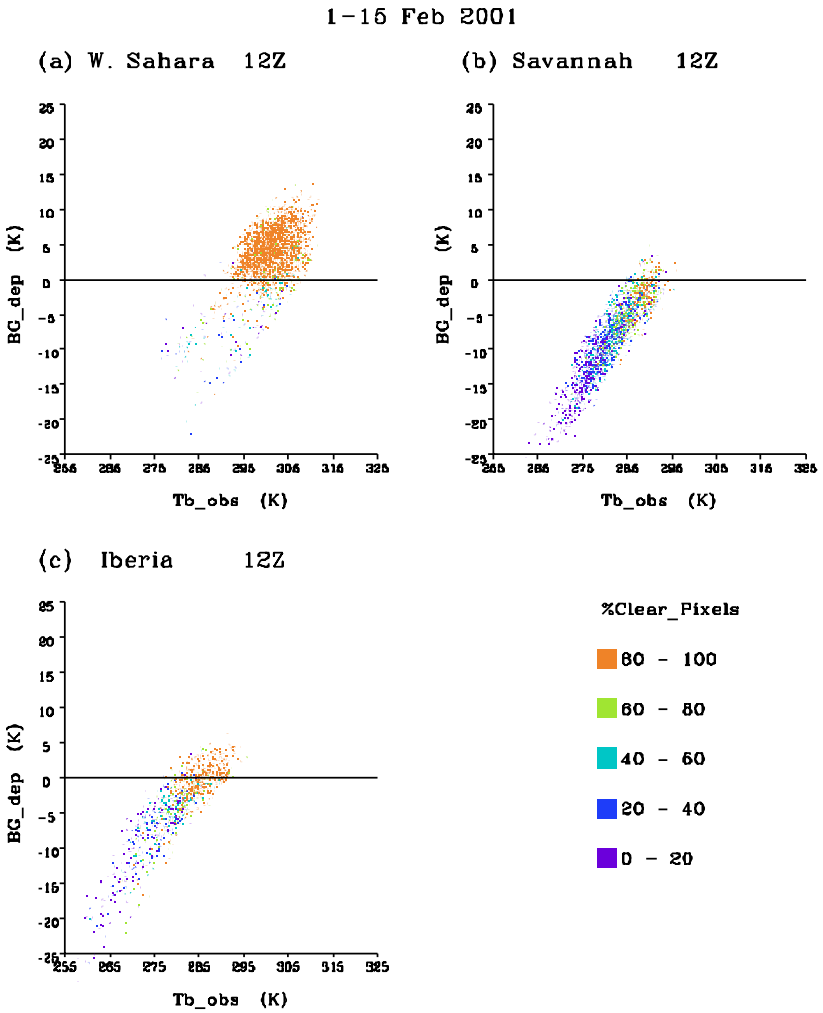

Figure 10 Scatterplots of the BG_dep (K) against Tb_obs (K), for (a) Western Sahara, (b) Savannah, and (c) Iberian Peninsula at 12 UTC. The points are colored according to the percent of clear-sky pixels taken into account for each observation.

The frequency of the daily maximum of Tb_obs for Iberia, Mali and the Savannah limited areas is shown in Fig. 11 for (1) and in Fig. 12 for (2). Here we assume that a high water vapor content would decrease the daily amplitude of Tb_obs (e.g., Yang and Slingo 2001), but have a negligible impact on the phase of the diurnal cycle. As expected, for the cases shown in Fig. 12 Tb_obs peaks essentially between 12 UTC and 15 UTC, 1-2 hours after the solar maximum. Differences in the peak times reflect mainly the longitude of the different areas.

The histograms shown in Fig. 11 also tend to exhibit maximum frequencies for 12-15 UTC. However, the spreading of daily maxima through all observation times points very strongly to the influence of clouds. The most uniform distributions are generally found for midlatitudes (see Iberia in Fig. 11), in accordance with the lack of any particular diurnal cycle associated with frontal systems that may affect the regions. For the Mali and Savannah limited areas, the maximum values of Tb_obs tend to be more spread during the peak of the

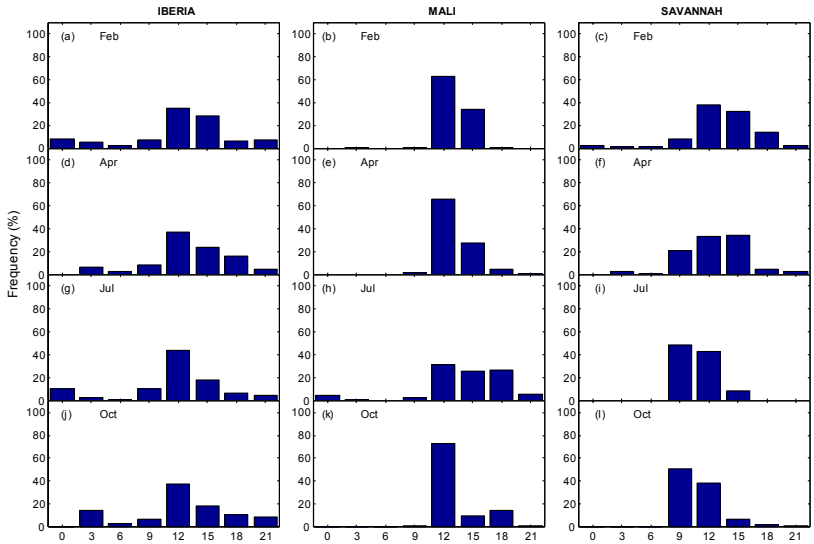

Figure 11 Distribution of the daily maximum of Tb_obs for Iberia (1st column), Mali (2nd column) and Savannah (3rd column) limited areas, when the daytime (12 or 15 UTC) BG_dep is lower than –5K and the model fraction of total cloud cover is higher than 0.5. The histograms are shown for 15-day periods in February, April, July and October.

rainy season, in July (Fig. 11h) and February (Fig. 11c), respectively. The results are consistent with the diurnal cycle of convection in the two regions; over the Savannah limited area there is a strong tendency for convection to occur by late afternoon (Yang and Slingo 2001), when Tb_obs daily maxima are less frequent. Over west Africa, including the Mali, the influence of mesoscale convective systems is less localized than for the case of the Savannah (e.g. Gray and Jacobson 1977; Hodges and Thorncroft 1997; Yang and Slingo 2001), and daily Tb_obs maxima are further spread through the afternoon (Fig. 12h).

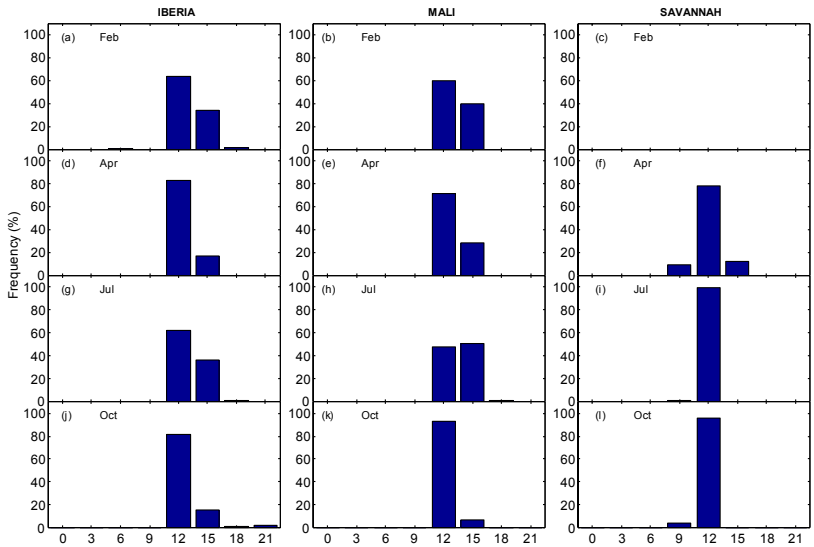

Figure 12 As in Fig. 11, but for cases with daytime (12 or 15 UTC) positive BG_dep and modeled fraction of total cloud cover lower than 0.5.

5. Conclusions

The comparison between modeled and observed top of the atmosphere radiances presented here has two main purposes: the identification of problems with the observational data and the assessment of the model quality. Under clear sky conditions, the diurnal cycle of the window channel brightness temperatures, and thus of land surface temperature, tends to be greatly underestimated by the model, particularly over arid and semi-arid land areas. Similar problems exist for comparison with the window channel of the TOVS instrument (Tony McNally, private communication). This poses strong limitations to the assimilation of information from channels from polar obiter sounders, sensitive to the lower troposphere. The assimilation of such channels will only be possible after reducing substantially the uncertainties of the surface temperature background fields, which may be achieved in two steps by: (1) reviewing the surface parameters prescribed in TESSEL, aiming to eliminate most of the systematic errors of the model surface temperature; and (2) introducing 1D-Var assimilation of window channel radiances to correct random errors of the background land surface field before starting the 4D-Var process.

The use of currently available Meteosat data for assimilation of land surface variables requires care in handling clear-sky observations. The current operational cloud processing for Meteosat is limited by the reduced number of channels available. However, the results shown in Fig. 10 suggest that the problem may be temporarily solved by flagging "cloud contaminated" observations, i.e. requiring a minimum value of the respective %_ClearSky (e.g. 75%). The instruments on-board Meteosat Second Generation (MSG) will have considerably more channels (12) and a higher spatial and temporal resolution, which will allow the use of more accurate cloud processing algorithms (Lutz 1999).

Recent sensitivity experiments suggest modifications to TESSEL surface parameters (e.g. roughness length for heat), in line with information from previous field experiments (Malhi 1996). We expect to update those parameters, directly associated with surface-to-atmosphere coupling, so that the model-observations discrepancies described here for clear-sky conditions may be corrected. The main purpose of such exercise will be to enable a first assessment of the usage of lower tropospheric channels in polar orbiters (currently operational only over sea) extended to land surfaces.

Acknowledgements

The kind help and discussions with Anton Beljaars, Frederic Chevallier, Graeme Kelly, Christina Köpken, Tony McNally, and Jean-Noël Thépaut helped to focus this work and shape this manuscript, and is greatly appreciated. The first author is funded by the Land Surface Analysis Satellite Application Facility (LSA SAF), co-sponsored by the European Organization for the Exploitation of Meteorological Satellites. The authors are also grateful to Carlos DaCamara, scientific coordinator of LSA SAF, for his helpful comments. The work reported in this paper was performed during a visit of the first author to ECMWF.

References

Bouttier, F., 2001: The development of 12-hourly 4D-VAR. ECMWF Tech. Mem. 348, 21pp.

Bouttier, F., and G. Kelly, 2001: Observing systems experiments in the ECMWF 4D-Var data assimilation system. *Quart. J. Roy. Meteor. Soc.*, **127**, 1469-1488.

Chang, H.-D., P. H. Wang, T. T. Wilheit, A. T. C. Chang, D. H. Staelin, and P. W. Rosenkranz, 1984: Monthly distributions of precipitable water from the NIMBUS-7 SMMR data. *J. Geophys. Res*., **89**, 5328-5334.

Chevallier, F., P. Bauer, G. Kelly, C. Jakob, and T. McNally, 2001: Model clouds over oceans as seen from space: comparison with HIRS/2 and MSU radiances. *J. Climate*, **14**, 4216-4229.

Chevallier, F., and G. Kelly, 2002: Model clouds as seen from space: comparison with geostationary imagery in the 11mm window channel. *Mon. Wea. Rev*., **130**, 712-722.

Deardorff, J.W., 1978: Efficient prediction of ground surface temperature and moisture, with inclusion of a layer of vegetation. *J. Geophys. Res*., **83C**, 1889-1903.

Dickinson, R.E., A. Henderson-Sellers, C. Rosenzweig, and P.J. Sellers, 1991: Evapotranspiration models with canopy resistance for use in climate models, a review. *Agric. For. Meteorol*., **54**, 373-388.

Dickinson, R.E., A. Henderson-Sellers, and P.J. Kennedy, 1993: Biosphere-atmosphere transfer scheme (BATS) Version 1E as coupled to the NCAR community model. NCAR Technical Note, NCAR/TN-387, 72 pp.

Eyre, J. R., 1991: A fast radiative transfer model for satellite sounding systems. ECMWF Tech. Memo. No. 176, 28 pp.

Gray, W. M., and R. W. Jacobson, 1977. Diurnal variation of deep cumulus convection. *Mon. Wea. Rev*., **105**, 1171-1188.

Hall, F.G., K. F. Huemmrich, S.J. Goetz, P.J. Sellers, and J.E. Nickeson, 1992: Satellite remote sensing of surface energy balance: Success, failures, and unresolved issues. *J. Geophys. Res*., **97D**, 19,061-19,089.

Hodges, K. I., and C. D. Thorncroft, 1997. Distribution and statistics of African mesoscale convective weather systems based on the ISCCP Meteosat imagery. *Mon. Wea. Rev*., **125**, 2821-2837.

Jakob, C., 1999: Cloud cover in the ECMWF reanalysis. *J. Climate*, **12**, 947-959.

Jakob, C., and S. A. Klein, 2000: A parameterization of the effects of cloud and precipitation overlap for use in general-circulation models. *Q. J. Roy. Meteor. Soc*., **126**, 2525-2544.

Jakob, C., E. Andersson, A. Beljaars, R. Buizza, M. Fisher, E. Gérard, A. Ghelli, P. Janssen, G. Kelly, A. P. McNally, M. Miller, A. Simmons, J. Teixeira, and P. Viterbo, 2000: The IFS cycle CY21r4 made operational in October 1999. ECMWF Newsletter, 87, 2-9.

Jin, M., R. E. Dickinson, and A. M. Vogelmann, 1997: A comparison of CCM2-BATS skin temperature and surface-air temperature with satellite and surface observations. *J. Climate*, **10**, 1505-1524.

Joyce, R., J. Janowiak, and G. Huffman, 2001: Latitudinally and seasonally dependent zenith-angle corrections for geostationary satellite IR brightness temperatures. *J. Appl. Meteor*., **40**, 689-703.

Klinker, E., F. Rabier, G. Kelly, and J.-F. Mahfouf, 2000: The ECMWF operational implementation of four-dimensional variational assimilation. I: Experimental results and diagnostics with operational configuration. *Q. J. Roy. Meteor. Soc*., **126**, 1191-1215.

Köpken, C., 2001: Monitoring of ECMWF WV radiances and solar stray light effects. EUMETSAT/ECMWF Fellowship Report No. 10, 46 pp.

Köpken, C., G. Kelly, and J.-N- Thépaut, 2002: Monitoring and assimilation of Meteosat radiances within the 4DVAR system at ECMWF. EUMETSAT/ECMWF Fellowship Report No. 9, 31 pp.

Loveland, T.R., B.C. Reed, J.F. Brown, D.O. Ohlen, J. Zhu, L. Yang, and J.W. Merchant, 2000: Development of a Global Land Characteristics database and IGBP DISCover from 1-km AVHRR data. *Int. J. Remote Sens*., **21**, 1303-1330.

Lutz, H.-J., 1999. Cloud processing for Meteosat second generation. EUMETSAT Technical Memorandum No. 4, 26 pp.

Mahfouf, J.-F., and F. Rabier, 2000: The ECMWF operational implementation of four-dimensional variational assimilation. I: Experimental results with improved physics. *Q. J. Roy. Meteor. Soc*., **126**, 1171-1190.

Malhi, Y., 1996. The behaviour of the roughness length for temperature over heterogeneous surfaces. *Q. J. R. Meteorol. Soc*., **122**, 1095-1125.

Marécal, V., E. Gérard, J.-F. Mahfouf, and P. Bauer, 2001: The comparative impact of the assimilation of the SSM/I and TMI brightness temperatures in the ECMWF 4D-Var system. *Q. J. Roy. Meteor. Soc*., **127**, 1123-1142.

Marécal, V., and J.-F. Mahfouf, 2002: Four-dimensional assimilation of total column water vapor in rainy areas. *Mon. Wea. Rev*., **130**, 43-58.

Matricardi, M., F. Chevallier, and S. Tjemkes, 2001: An improved general fast radiative transfer model for the assimilation of radiance observations. ECMWF Tech. Memo. No. 345, 40 pp.

McNider, R.T., A.J. Song, D.M. Casey, P.J. Wetzel, W.L. Crosson, and R.M. Rabin, 1994: Towards a dynamic-thermodynamic assimilation of satellite surface temperature in numerical atmospheric models. *Mon. Wea. Rev*., **122**, 2784-2803.

Morcrette, J.-J., 1991: Evaluation of model-generated cloudiness: satellite-observed and model-observed diurnal variability of brightness temperature. *Mon. Wea. Rev*., **119**, 1205-1224.

Morcrette, J.-J., 2002: Assessment of the ECMWF model cloudiness and surface radiation fields at the ARM-SGP site. *Mon. Wea. Rev*., **130**, 257-277.

Munro, R., G. Kelly, and R. Saunders, 2000. Assimilation of Meteosat radiance data within the 4DVAR system at ECMWF. EUMETSAT/ECMWF Fellowship Report No. 8.

Rabier, F., H. Järvinen, E. Klinker, J.-F. Mahfouf, and A. Simmons, 2000: The ECMWF operational implementation of four-dimensional variational assimilation. I: Experimental results with simplified physics. *Q. J. Roy. Meteor. Soc*., **126**, 1143-1170.

Reynolds, R.W., and T.M. Smith, 1994: Improved global surface temperature analyses using optimum interpolation. *J. Climate*, **7**, 929-948.

Rhoads, J., R. Dubayah, D. Lettenmaier, G. O'Donell, and V. Lakshmi, 2001: Validation of land surface models using satellite-derived surface temperature. *J. Geophys. Res*., **106D**, 20,085-20,099.

Rohn, M., G. Kelly, and R. W. Saunders, 2001: Impact of new cloud motion wind product from Meteosat on NWP analyses and forecasts. *Mon. Wea. Rev*., **129**, 2392-2403.

Saunders, R., M. Matricardi, and P. Brunel, 1999: An improved fast radiative transfer model for assimilation of satellite radiance observations. *Q. J. Roy. Meteor. Soc*., **125**, 1407-1425.

Sellers, P.J., R.E. Dickinson, D.A. Randall, A.K. Betts, F.G. Hall, J.A. Berry, G.J. Collatz, A.S. Denning, H.A Mooney, C.A Nobre, N. Sato, C.B. Field, A. Henderson-Sellers, 1997: Modeling the exchanges of energy, water, and carbon between continents and the atmosphere. *Science*, **275**,502-509.

Sellers, P.J., D.A. Randall, G.J. Collatz, J.A. Berry, C.B. Field, D.A. Dazlich, C.Zhang, G.D. Collelo, and L. Bounoua, 1996: A revised land surface parameterization (SiB2) for GCMs. Part I: Model formulation. *J. Climate*, **9**, 676-705.

Simmons, A. and A. Hollingsworth, 2002: Some aspects of the improvement in skill of numerical weather prediction. *Quart. J. Roy. Meteor. Soc*., **128**, 647-677.

Snyder, W. C., Z. Wan, Y. Zhang, and Y.-Z. Feng, 1998. Classification-based emissivity for land surface temperature measurement from space. *Int. J. Remote Sensing*, **19**, 2753-2774.

Sun, J., and L. Mahrt, 1995: Determination of surface fluxes from the surface radiative temperature. *J. Atmos. Sci*., **52**, 1096-1106.

Tiedtke, M., 1993: Representation of clouds in large-scale models. *Mon. Wea. Rev*., **121**, 3040-3061.

Tjemkes, S. A., M. König, H.-J. Lutz, and L. van de Berg, 2001: Calibration of Meteosat Water Vapor Channel observations with independent observations. *J. Geophys. Res*., **106D**, 5199-5209.

van de Berg, L., J Schmetz, and J. Whitlock, 1995: On the calibration of the Meteosat water vapor channel. *J. Geophys. Res*., **100D**, 21069-21076.

van den Hurk, B.J.J.M., P. Viterbo, A.C.M. Beljaars, and A.K. Betts, 2000: Offline validation of the ERA40 surface scheme. ECMWF Tech. Mem. 295, 42 pp.

Viterbo, P., and A.C.M. Beljaars, 1995: An improved land surface parameterization scheme in the ECMWF model and its validation. *J. Climate*, **8**, 2716-2748.

Wang, J.R., S.P. Goginegi, and J. Ampe, 1992: Active and passive microwave measurements of soil moisture in FIFE. *J. Geophys. Res*., **97D**, 18,979-18,985.

Yang, G.-Y., and J. Slingo, 2001: The diurnal cycle in the tropics. *Mon. Wea. Rev*., **129**, 784-801.